RSC Advances

PAPER

View Article Online
View Journal | View Issue



Cite this: *RSC Adv.*, 2025, **15**, 37299

# Photochemical valorization of hydrogen sulfide: a study of UV-induced decomposition pathways

Hassnain Abbas Khan, [a] Ali Elkhazraji,[bc] Mohammad Abou-Daher, [a] Damian P. San Roman Alerigi, [d] Khalid Hazazi[d] and Aamir Farooq *[a]

Hydrogen sulfide ($H_2S$) is a toxic and environmentally hazardous gas, yet it also represents a potential source of valuable hydrogen. This study investigates the direct gas-phase decomposition of $H_2S$ into hydrogen ($H_2$) and elemental sulfur ($S_x$) using UV-C light sources through both photolytic and photocatalytic pathways. Experiments were conducted using a 220 nm UV laser and a 254 nm mercury (Hg) lamp in distinct reactor configurations. Photolysis of 5% $H_2S/N_2$ achieved conversion efficiencies of up to 44% and 52% within 60 minutes using the laser and Hg lamp, respectively. In flow experiments (space velocity ~15 $h^{-1}$), conversion decreased to 13–16%. In both static and flow modes, sulfur deposition on optical surfaces hindered UV transmission, thereby reducing overall efficiency. Incorporating a CuS photocatalyst significantly enhanced $H_2S$ decomposition, reaching 66% conversion under UV-C illumination. X-ray photoelectron spectroscopy (XPS) confirmed the presence of mixed $Cu^{+}/Cu^{1+\delta}$ valence states in CuS, enabling localized surface plasmon resonance (LSPR) that promotes charge separation and catalytic activity. These findings underscore the promise of UV-C-driven $H_2S$ splitting as a sustainable approach for hydrogen and sulfur co-production, offering a cleaner alternative to conventional treatment methods.

Received 15th June 2025
Accepted 26th September 2025

DOI: 10.1039/d5ra04250j

rsc.li/rsc-advances



## 1. Introduction

Hydrogen sulfide ($H_2S$) is recognized as a noxious gas that poses significant environmental and health risks due to its toxic nature; for example, its odor threshold ranges between 0.4 ppb and 1.5 ppm.[1] Exposure to concentrations as low as 100 ppm is highly toxic and can lead to death within 48 hours, while levels exceeding 700 ppm are fatal within minutes.[2] $H_2S$ is naturally abundant in crude oil and natural gas well sites.[3] Its oxidation can form sulfur oxides, which pose significant health and environmental risks and cause severe corrosion.[4] Downstream, stringent treatments (pre-/post-combustion) are necessary in refineries and power plants to control the emissions of sulfuric pollutants (*i.e.*, $H_2S$, $SO_x$).[5,6]

Various methods are currently used to capture and eliminate $H_2S$. The most common techniques include solubilization in an aqueous basic media[7] and the Claus process.[8] The latter is widely utilized in industry due to its economic viability and established operation framework. It involves a two-step reaction.[8] Initially, $H_2S$ undergoes thermal oxidation above 1000 °C to produce sulfur dioxide ($SO_2$) and water at elevated temperatures. Then, a catalytic step employing activated aluminum(III) or titanium(IV) oxides converts the remaining $H_2S$ and $SO_2$ to elemental sulfur and water. The process can achieve a conversion efficiency of up to 98%, leaving about 2–5% of $H_2S$ unconverted as tail gas.[9–11] This residual $H_2S$ poses environmental and safety concerns, as it is a toxic and malodorous gas.[12] Hence, additional purification steps are necessary to remove this residual $H_2S$,[13,14] including catalytic oxidation or absorption processes, which add complexity and cost to the overall operation.[15,16] Furthermore, the presence of contaminants in the feed gas, such as aromatic compounds (*e.g.*, benzene, toluene, and xylenes) can affect the reaction kinetics[17] and lead to catalyst deactivation and the formation of soot, which clogs the catalytic reactors and reduces their efficiency,[18] From the perspective of energy intensity, the need for high temperatures to facilitate the reaction also contributes to increased energy consumption and operational costs.[19,20] These limitations pose significant challenges that demand the development of novel alternatives for $H_2S$ decomposition that are energy-efficient and sustainable.

Considering these limitations, researchers have explored alternative methods for $H_2S$ treatment and removal[21–23] Recent research endeavors have focused on harnessing $H_2S$ as a source

[a]*Clean Energy Research Platform, Physical Sciences and Engineering Division, King Abdullah University of Science and Technology (KAUST), Thuwal 23955-6900, Kingdom of Saudi Arabia. E-mail: aamir.farooq@kaust.edu.sa*

[b]*Department of Mechanical Engineering, King Fahd University of Petroleum & Minerals, Dhahran 31261, Saudi Arabia*

[c]*Interdisciplinary Research Center for Hydrogen Technologies and Carbon Management, King Fahd University of Petroleum & Minerals, Dhahran 31261, Saudi Arabia*

[d]*Exploration and Petroleum Engineering Center-Advanced Research Center (EXPEC ARC), Saudi Aramco, Dhahran 34465, Saudi Arabia*

of hydrogen ($H_2$).[23,24] Such a paradigm shift would eliminate $H_2S$ while positioning it as a contributor to the hydrogen economy. Several methods of producing hydrogen from $H_2S$ have been described in the literature, including thermal,[25] electrochemical,[26] plasma-chemical,[27] and photocatalytic.[28–32] However, many of these methods suffer from the overoxidation of elemental sulfur, leading to the formation of toxic sulfite and sulfate-bearing compounds. Light-driven methods are of particular interest because of the abundance of sunlight and the continuous improvement in the efficiency of light-emitting diodes. Several studies have studied the photo-physics of the H–S bond under the UV, visible, and IR spectra[12,33,34] to uncover light's potential as a driving force for $H_2S$ decomposition. However, the gas-phase splitting of $H_2S$ to produce hydrogen and elemental sulfur and the nature and yields of these reaction products have not been explored in depth. From a practical perspective, the design of reactors for gas-phase photolysis and photocatalysis is critical for optimizing contact time and light exposure.

Solar light offers significant advantages as an energy source for several reasons. One key benefit is that photon energy can be transferred directly to the molecules without any external power input; the only requirement is a transparent matrix at the excitation wavelength.[35] Additionally, advanced technologies enable the filtering of the solar light spectrum to isolate specific wavelengths, such as UV, visible, or IR, tailored to particular applications. This capability enhances the versatility and efficiency of solar energy utilization. Recent studies have explored the photodecomposition of $H_2S$ into hydrogen gas in the liquid phase using semiconductor and noble metal co-catalysts under UV/vis light irradiation.[36] The combination of UV-C (200–280 nm) and VUV (<200 nm, typically 172 nm from Xe excimer lamps) radiation has been shown to significantly enhance the degradation rates of $H_2S$, suggesting that advanced oxidation processes (AOPs) can be effectively employed for this purpose.[37,38] Some studies have utilized air as an intermediary to decompose $H_2S$, though achieving net-zero sulfur remains elusive with this approach.[39] These studies often utilized low concentrations of $H_2S$, resulting in the formation of sulfur-containing acids that can cause photocatalyst deactivation. While non-oxidative gas-phase $H_2S$ splitting has received limited attention, it holds great promise for the simultaneous production of hydrogen and elemental sulfur.[21,40] The non-oxidative photochemical approach shows minimal to no interference of other gases, such as $CO_2$, $CH_4$, and $N_2$, present in natural gas streams.[40]

This study investigates the efficiency of direct gas-phase $H_2S$ splitting under UV-C irradiation, both photolytically and photocatalytically. Specifically, the study explores two UV-C wavelengths (220 nm and 254 nm) due to the high absorption cross-section of $H_2S$ at 220 nm and the more significant solar flux at longer (254 nm) wavelengths. Instead of directly using solar radiation, this work utilizes a laser source at 220 nm and a lamp at 254 nm. Applying a light source at 220 nm, seldom investigated in the literature, is a significant contribution of this research. The results of this work will help advance the technology of photochemical conversion of $H_2S$ to $H_2$ and S.

## 2. Experimental details

The current study uses two distinct UV sources and reactor systems: a Ti:sapphire laser system coupled to a metallic photoreactor, and a Mercury lamp embedded in a quartz photoreactor. The concentration of $H_2S$ ranges from 1% to 10%, and the decomposition behavior is investigated from ambient temperature (25 °C) to elevated temperature (125 °C) at a pressure of ~1.5 bar. The $H_2S$ gas cylinders with purity levels (1–10% in $H_2S$ nitrogen) are sourced from Gulf Gas Corporation Saudi Arabia. The feed gases $H_2S/N_2$ flowed through the reactor, and the effluents were introduced into a Thermo Fisher scientific gas chromatograph (GC) equipped with two TCD detectors and an Rtx-1 and $Al_2O_3$–$Na_2SO_4$ double-column separation system for the reactivity measurements. A calibration curve was applied to quantify the $H_2S$ and $H_2$ signals. The condensation of sulfur powder could also be observed visually during the decomposition and recorded with a camera. The sulfur is analyzed with X-ray diffraction to identify the phase-type and purity.

### 2.1. Ti:sapphire laser system coupled to a metallic photoreactor

The Praying Mantis™ high-temperature (Harrick Scientific Products) reactor (20 ml volume) with a modified dome is used in this study. The reactor has three UV-grade optical windows for laser illumination with 99.5% UV transmission efficiency. Titanium-doped sapphire (Ti:sapphire) crystal generates the desired wavelength. Ti:sapphire is a solid-state laser medium capable of tunable operation over a broad range of near-infrared (IR) wavelengths. Here, we used a mode-locked laser (Tsunami®), which gave tunable output over 690 nm to 1080 nm. The laser was operated at a repetition rate of 80 MHz and a pulse width of 2 ps. The Ti:sapphire laser was pumped by a 532 nm Nd:YAG diode-pumped solid-state laser (Millennia®). The near-IR photons were upconverted to UV through two consecutive second harmonic generation processes, equivalent to fourth harmonic generation (FHG). Fig. 1 shows a schematic of the optical setup used to test when the laser is used as a laser source coupled with a metallic photoreactor.

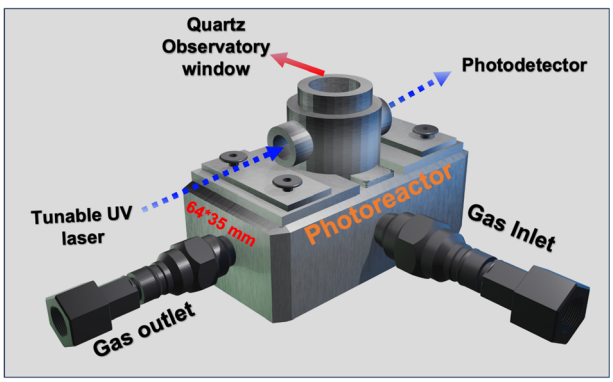


Fig. 1 Schematic of the photolysis setup using a modified Harrick photoreactor.

### 2.2. Mercury lamp coupled to a quartz photoreactor

This study used a double-tube UV-grade quartz reactor and UV lamp. The reactors geometry is shown in Fig. 2. The $H_2S$ flows through 20 ml volume outer tube. The UV source, a mercury (Hg) lamp (*Ushio G8T5*), is located inside the inner tube and illuminates the reactor directly. This lamp emits a quasi-monochromatic light at 254 nm with an output power of 2.5 W.

## 3. Results and discussion

### 3.1. Photolysis of $H_2S$ at 220 nm

Fig. 3 shows the photodecomposition of $H_2S$ as a function of reaction time at a wavelength of 220 nm and an optical power of 12 mW. These experiments were carried out in a batch mode using the metallic photoreactor with three mixtures of varying $H_2S$ concentrations. These data clearly show the increasing conversion of $H_2S$ as a function of illumination (or reaction) time. Conversions of 35%, 27%, and 18% are recorded for the 1%, 5%, and 10% $H_2S$ mixtures, respectively, after 30 minutes of reaction time. These results indicate the rapid initiation of the photodecomposition process. As the light exposure time progresses, the conversion of $H_2S$ steadily increases, reaching almost 94%, 44%, and 36% at 60 minutes and rising to 96%, 89%, and 76% at 120 minutes for the 1%, 5%, and 10% $H_2S$ mixtures, respectively. Nearly complete removal of $H_2S$ is observed after 180 minutes for the 5% $H_2S$ mixtures, while more than 90% conversion is observed for the 10% $H_2S$ mixture.

The plots in Fig. 3 confirm the conversion rates follow an exponential decay, typical of first-order reactions, with a rate constant inversely proportional to the initial concentration. The cause of this reduced reactivity is likely due to the condensation of sulfur on the optical windows, which inhibits the transmission of light inside the cavity. This effect was confirmed using a photodetector placed downstream of the reactor to quantify the transmitted laser intensity, which was found to decline with the thickening of the sulfur layer forming on the optical windows, as shown in Fig. S1 (SI). The condensation of sulfur powder produced from photolyzed $H_2S$ was recorded using an HD camera (see Fig. S2). Sulfur powder condensation was observed on the optical windows soon after the laser beam was propagated through the reactor. As shown in Fig. S2, the initial frame at time 0 reveals clear optical windows. Within only 2 seconds, the distinct appearance of sulfur becomes evident on the optical windows. As the reaction progresses, the sulfur layer thickens and eventually covers substantial portions of the optical windows. The time-lapse recording provides an insightful visual representation of the rapidity with which the reaction proceeds, thereby highlighting the swift onset of sulfur formation. The emergence of sulfur indicates the complete dissociation of $H_2S$ molecules to hydrogen and sulfur (rather than SH + H formation). We have provided a video recording as SI for visualizing the instant $H_2S$ decomposition and sulfur formation.

Fig. 4 shows the impact of optical power on the efficiency of the photodecomposition process. The remarkable 89% conversion achieved with 25 mW of laser power at 220 nm wavelength during a 60-minute reaction is noteworthy. Increasing the laser power from 12 mW to 25 mW resulted in more than 2× increase in $H_2S$ conversion, indicating a non-linear effect of laser power on the conversion efficiency. Fig. 4 also shows the effect of reaction temperature on $H_2S$

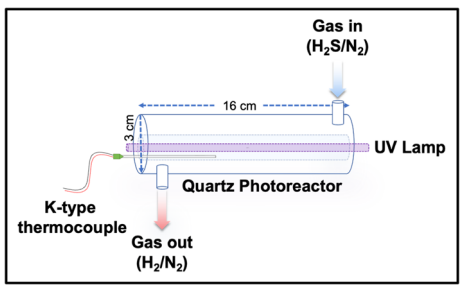


Fig. 2 Hollow jacketed quartz photoreactor for $H_2S$ photolysis.

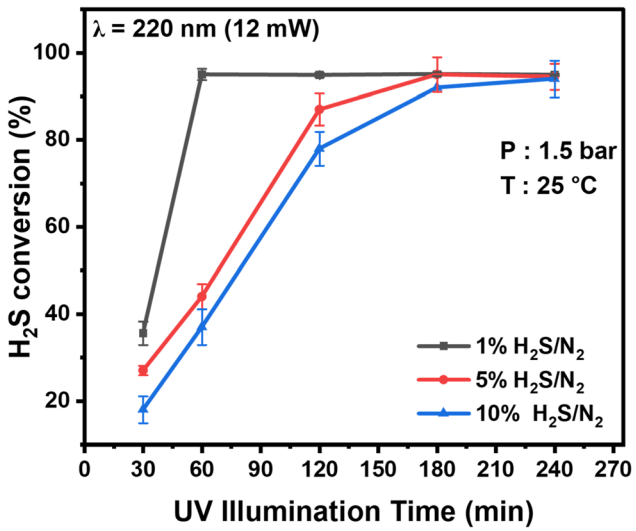


Fig. 3 Photolysis of $H_2S$ at 220 nm in the metallic photoreactor for different $H_2S/N_2$ mixtures as a function of reaction (UV illumination) time.

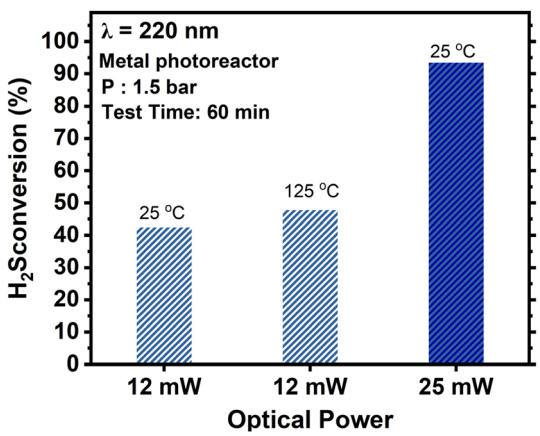


Fig. 4 Effect of laser power and reaction temperature on the photolysis of 5% $H_2S$ at 220 nm.

conversion. Increasing the temperature from 22 °C to 125 °C raised conversion from 42% to 49%. These findings emphasize the interplay between laser wavelength, optical power, temperature, reactor design and solid sulfur accretion, all of which governing $H_2S$ photodecomposition efficiency. The accumulation of sulfur significantly disrupts this process by obstructing light reaching the $H_2S$ molecules, scattering or attenuating incident photons.

### 3.2. Photolysis of $H_2S$ at 254 nm

This section discusses the results of $H_2S$ photodecomposition in the quartz reactor exposed to an Hg lamp emitting UV light at ~254 nm. The input electrical power of the UV lamp is 8 W and it emits 2.5 W optical power (data provided by Ushio Inc). Fig. 5 shows that gas mixtures containing 5% and 10% $H_2S$ result in nearly complete $H_2S$ conversions while yielding stoichiometric amounts of $H_2$ moles. Similar to the metal photoreactor experiments, sulfur condensed on the quartz reactor walls (see Fig. S3). Although the reactor was not externally heated in these experiments, the temperature inside the quartz reactor reached ~50 °C in 3 hours due to the heat dissipation from the Hg lamp.

The observed conversions at specific time intervals plotted in Fig. 5 reveal the progressive decomposition of $H_2S$ under the influence of UV irradiation. For the 10% $H_2S$ case, an initial conversion of 19.8% is measured after 30 minutes, reaching 51% after 60 minutes and 69% after 120 minutes. By 180 minutes, the conversion reaches nearly 97%, with the remaining $H_2S$ mole fraction being 0.27%. This result indicates the continued efficiency of the UV lamp in driving the dissociation of $H_2S$ over time. The decomposition rate is higher for the 5% $H_2S$ case than for the 10% $H_2S$ case. The initial conversion at 30 minutes is 24%, and the conversion reaches 82% in 120 minutes. The quartz reactor becomes entirely covered with sulfur powder (see Fig. S3), confirming the $H_2S$ decomposition process in 60 minutes. This change in transparency due to sulfur accumulation before and after the reaction is a tangible indication of effective $H_2S$ conversion under the UV light of the Hg lamp.

On the other hand, the reduced transparency results in lesser UV light transmission, which can explain the change in reaction rate and efficiency of the process. As a result, at later reaction times, the reaction rate is slower than at earlier illumination times. This observation highlights the need to develop sulfur removal and quenching techniques to improve the efficiency of the process.

### 3.3. Conversion efficiency

The efficiency of the photolytic process, in terms of moles of $H_2S$ converted per joule of optical energy, is calculated as follows:

$$\text{Conversion efficiency} = \frac{\text{Moles of } H_2S \text{ converted}}{E_{\text{total}}}$$

Fig. 6 presents an approach to evaluate the efficiency of photolysis process as the conversion of $H_2S$ moles per joule of optical power. The calculations are based on effective optical power (based on the optical access area of the reactor). The photolysis conversion efficiency, based on moles of $H_2S$ converted per joule of optical energy, was $8.54 \times 10^{-7}$ at 220 nm and $4.4 \times 10^{-9}$ at 254 nm, highlighting the superior performance at 220 nm.

Fig. 7 shows $H_2S$ conversion in continuous flow experiments in the quartz reactor. The procedure adopted here is batch-to-flow transition. The 5% $H_2S$ mixture is filled in the reactor, and the Hg lamp is illuminated to initiate the reaction. A continuous flow (5 ml $min^{-1}$) of 5% $H_2S$ mixture is initiated by controlling the outlet valve, resulting in a residence time of 240 s. Gas samples are collected every 12 min and analyzed using an online GC. The flow reactions were carried out over 350 minutes at room temperature (25 °C) and heated (125 °C) conditions. The reactor was heated using a heating tap, and the temperature of the reactor surface was measured using a K-type thermocouple. It is observed that the activity under the room temperature condition experienced a conversion reduction from ~13% to ~7%. Meanwhile, under the heated condition (125 °C), the activity remained stable throughout the

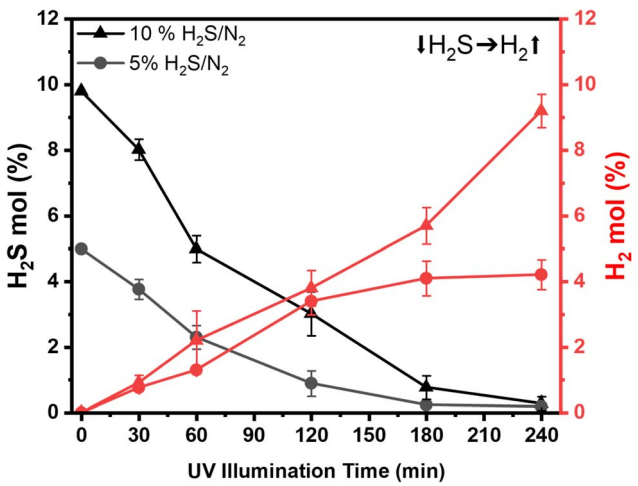


Fig. 5 Photolysis of two different mixtures of $H_2S/N_2$ in the quartz reactor using an Hg lamp emitting UV light at 254 nm.

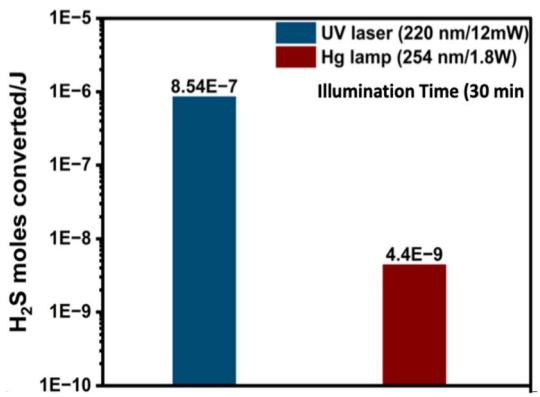


Fig. 6 $H_2S$ conversion efficiency per joule of optical power at 220 nm and 254 nm.

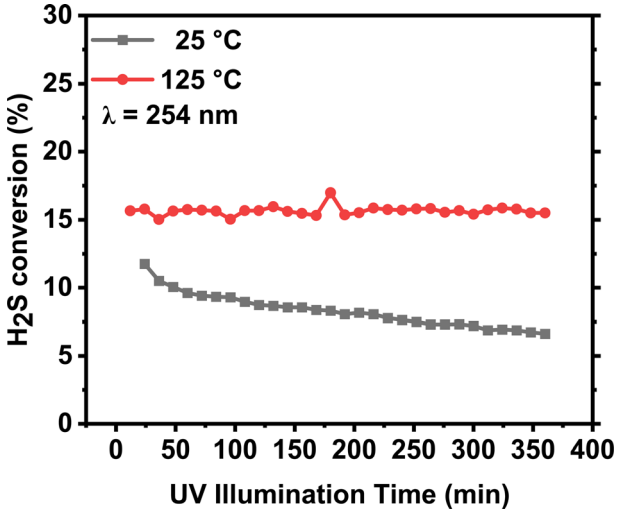


Fig. 7 $H_2S$ conversion in flow experiments in a quartz reactor using an Hg lamp at a GHSV (gas hourly space velocity) = 15 $h^{-1}$ at 25 °C and 125 °C.

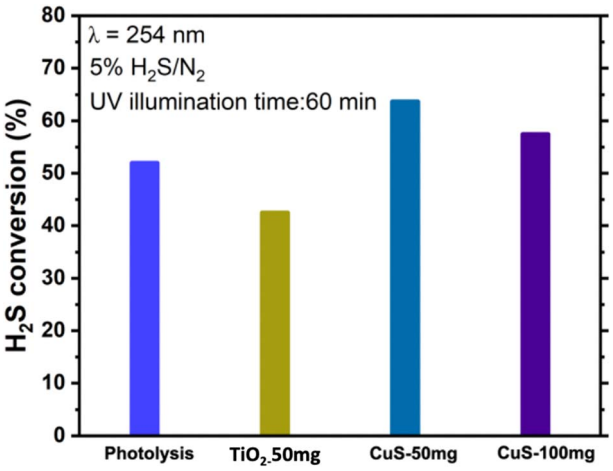


Fig. 8 Comparison of photolytic and photocatalytic batch experiments conducted in the quartz reactor with an Hg lamp.

experiment. At room temperature, the photoreactor became nearly opaque due to sulfur deposition after a 60-minute continuous reaction, significantly reducing UV light transmission and resulting in slower $H_2S$ conversion. Fig. S4 shows pictures of the reactor after the reaction. In the heated experiments, sulfur was observed only in the colder edges of the reactor during and after the reaction. This observation suggests that sulfur started to melt at 125 °C and condensed in the colder parts of the reactor.

### 3.4. Photocatalytic $H_2S$ decomposition

To understand the role of common catalysts in $H_2S$ conversion, two catalysts, namely commercial $TiO_2$ (CristalACTiV™ G5 supplied by Tronox, anatase phase) and an in-house synthesized CuS, were loaded into the quartz reactor by making stable suspension. Details about the synthesis method and catalyst characterizations are given in the SI. The performance of $TiO_2$ and CuS is assessed at various loadings and tested over 40–60 minutes in the quartz reactor. Fig. 8 plots the conversion rate for the photolysis and photocatalysis experiments. The results show that the $TiO_2$ catalyst did not improve $H_2S$ decomposition compared to the photolytic reaction. It is important to note that $TiO_2$ started to turn yellowish as soon as the reaction began. It is speculated that the formed sulfur resulted in $TiO_2$ poisoning. In the case of CuS, a higher rate of reaction was achieved compared to the photolytic reaction, likely due to the plasmonic effect. However, as the quantity of the CuS catalyst in the reactor was increased to 100 mg *via* multiple coatings, the activity slightly decreased due to the reduced UV light transmission. This result suggests that the effective transmission of UV light is crucial for $H_2S$ photolytic and photocatalytic decomposition.

Table S1 (SI) benchmarks our results against relevant literature on $H_2S$ photolysis and photocatalysis. Previous gas-phase studies by Baldovi *et al.* (2017),[40] achieved ~40% conversion at 254 nm without a catalyst, while $TiO_2$-based systems suffered from sulfur poisoning and showed limited efficiencies of 30–52% under UV-C illumination.[39,41] Aqueous-phase CuS photocatalysis demonstrated ~58% conversion under visible light,[28] but direct gas-phase application remained unexplored. In contrast, our work demonstrates for the first time that CuS achieves 66% $H_2S$ conversion in the gas phase under 254 nm irradiation, outperforming both $TiO_2$ benchmarks and photolysis alone. This establishes the novelty of our study in advancing gas-phase photochemical $H_2S$ valorization, bridging fundamental plasmonic behavior with practical conversion performance.

XRD analysis confirmed single-phase CuS in the pristine catalyst, while the spent catalyst showed additional reflections attributable to elemental sulfur deposition from $H_2S$ decomposition (Fig. S6). XRD patterns of $TiO_2$ confirmed a pure anatase phase, with no secondary phases detected after reaction. UV–vis diffuse reflectance spectra revealed a band gap of ~2.0 eV for CuS and 3.4 eV for pristine $TiO_2$, consistent with their photocatalytic activity. $TiO_2$ exhibited a red shift due to sulfur interaction (see Fig. S7).

Structural analysis was carried out using scanning electron microscopy (SEM) and transmission electron microscopy (TEM). SEM (Fig. 9a and b) and TEM (Fig. 9c and d) analyses show that the pristine CuS adopts a hierarchical plate-like architecture. In low-magnification SEM, micron-scale plates stack loosely, leaving inter-plate voids that form a porous network. At higher magnification, exposed edges and terraces are evident, consistent with the lamellar growth habit of covellite-type CuS. TEM further resolves ultrathin 2D nanosheets, a structural motif expected to (i) increase the accessible surface area and density of active edge sites, (ii) enhance internal light scattering within the stacked plate ensemble, and (iii) amplify local electromagnetic fields at sharp features, conditions favorable for localized surface plasmon resonance (LSPR) in p-type copper sulfides. For comparison, SEM and TEM images of $TiO_2$ are provided in Fig. S8, where high-resolution TEM highlights its highly porous morphology.

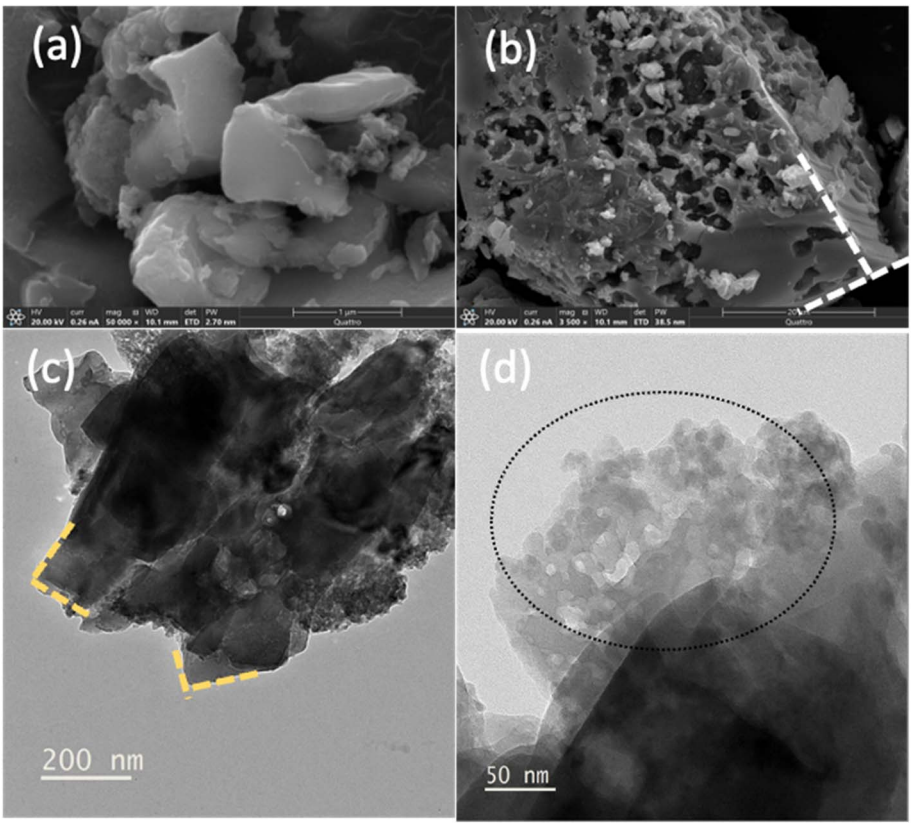


Fig. 9 (a and b) SEM showing stacked plate-like CuS with inter-plate porosity and exposed edges. (c) TEM of an ultrathin nanosheet plate highlighting thin edge regions. (d) Higher-magnification TEM revealing nano crystallites.

The surface chemical states of the synthesized CuS catalyst were investigated by X-ray photoelectron spectroscopy (XPS) to elucidate the nature of active species responsible for photocatalytic $H_2S$ decomposition. High-resolution spectra of Cu 2p, S 2p, and O 1s regions were recorded and deconvoluted to distinguish contributions from different oxidation states and surface species. The Cu 2p spectrum (Fig. 10a) displays two principal peaks at 931.7 eV (Cu $2p_{3/2}$) and 951.5 eV (Cu $2p_{1/2}$), assigned predominantly to $Cu^+$ species. Notably, the absence of shake-up satellite features in the 940–945 eV region, thereby confirming the covellite-type CuS phase as the dominant surface state.[42,43] Quantitative analysis shows the S $2p_{3/2}$ peak (Fig. 10b) at 161.7 eV (53.91% area) and a secondary S $2p_{1/2}$ at 162.8 eV (29.96% area), indicative of sulfide ions ($S^{2-}$) and minor surface-bound sulfur ($S^0$), respectively. The $SO_4^{2-}$ signal at 167.9 eV (19.13%) points to trace oxidation, likely due to ambient exposure. The absence of pronounced $Cu^{2+}$ satellite features in the Cu 2p region further substantiates the

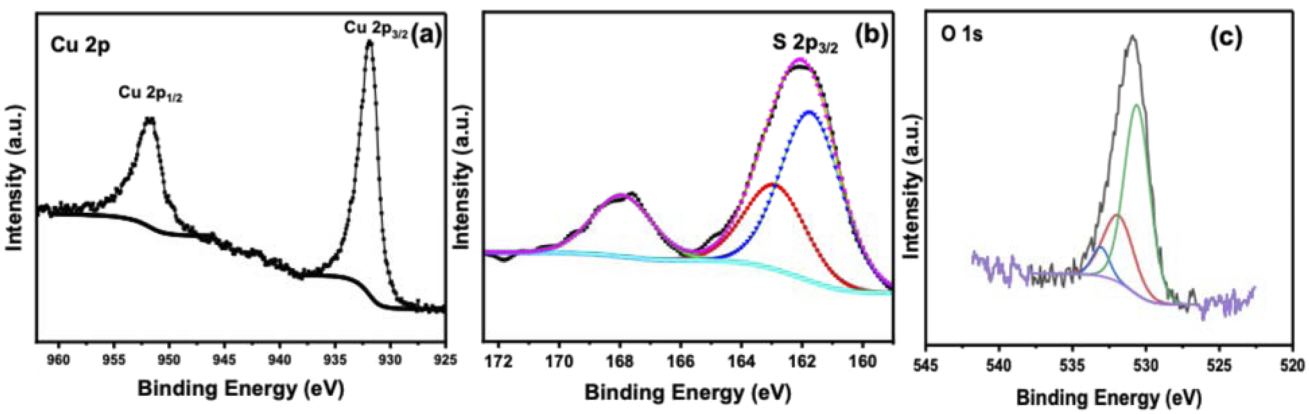


Fig. 10 High-resolution XPS spectra of CuS: (a) Cu 2p region showing Cu valence states, (b) S 2p region confirming $S^{2-}$ and surface $S^0$ species, and (c) O 1s region indicating adsorbed hydroxyl groups and minor surface oxygen species.

dominance of $Cu^{+}$ and confirms minimal surface oxidation. This electronic structure supports a robust LSPR (localized surface plasmon resonance) response, arising from the mixed-valence states and copper vacancies endemic to covellite, and thus facilitates effective charge separation and high photocatalytic activity under UV illumination.[44]

The O 1 s spectrum (Fig. 10c) displays a weak peak at ~531.5–532.5 eV, corresponding to adsorbed hydroxyl groups ($OH^{-}$) or molecularly physiosorbed water.[45] The absence of strong lattice oxygen signals indicates minimal bulk oxidation of CuS. Surface hydroxylation may enhance $H_2S$ adsorption and facilitate proton-coupled electron transfer reactions without compromising the structural integrity of the catalyst.

The XPS spectra of spent CuS catalyst exhibits distinct changes in its XPS spectra (Fig. S9), signifying surface and compositional transformations. The primary Cu $2p_3/_2$ peak shifts to 932.8 eV and Cu $2p_1/_2$ to 952.7 eV, reflecting mild oxidation or an increase in copper valency near the surface as a consequence of catalytic cycling. The S $2p_3/_2$ region also shifts upward to 162.7 eV (57.9% area), with the S $2p_1/_2$ peak at 163.9 eV (28.7% area), indicating a higher fraction of intermediate sulfur states. These binding energies are consistent with elemental sulfur ($S^0$) or polysulfide ($S_n^{2-}$) species, which are known to form during photocatalytic $H_2S$ decomposition. The contribution of sulfate ($SO_4^{2-}$, 168.8 eV) decreases to 13%, suggesting that surface species were partially consumed or removed during reaction, likely *via* transformation into lower-valence sulfur species or desorption under operating conditions. Such shifts in Cu and S binding energies are emblematic of dynamic surface processes that accompany robust photocatalytic activity. Notably, the persistence of a mixed-valence environment supports continued LSPR capability, though changes in surface composition may gradually impact efficiency and long-term stability.

Following the XPS characterization, a mechanistic model is proposed to correlate the surface chemical states of CuS with its photocatalytic performance under 254 nm illumination (Fig. 11). The UV photons (4.88 eV) possess energy greater than the CuS band gap (~2.1 eV), enabling efficient interband excitation of electrons from valence band (VB) to conduction band (CB). The XPS results confirms that Cu in CuS is predominantly in +1 oxidation state, with minor contributions from non-stoichiometric delocalized $Cu^{1+}\delta$ surface species consistent with copper deficit covellite type CuS. Such copper vacancies generate high hole densities that know to support plasmon resonance (LSPR), which further enhances charge carrier generation and separation.[46,47] Valence band holes ($h^{+}$) oxidize the adsorbed $H_2S$ molecules to protons ($H^{+}$) and elemental sulfur ($S^0$), while CB electrons and plasmonic hot electrons reduce the liberated protons to molecular hydrogen ($H_2$). Surface hydroxyl groups and sulfur species identified by XPS are likely to facilitate adsorption and proton-coupled electron transfer. Thus, the interplay of interband excitation and vacancy-induced plasmonic activity provides a synergistic pathway for efficient $H_2S$ decomposition into $H_2$ and $S^0$.

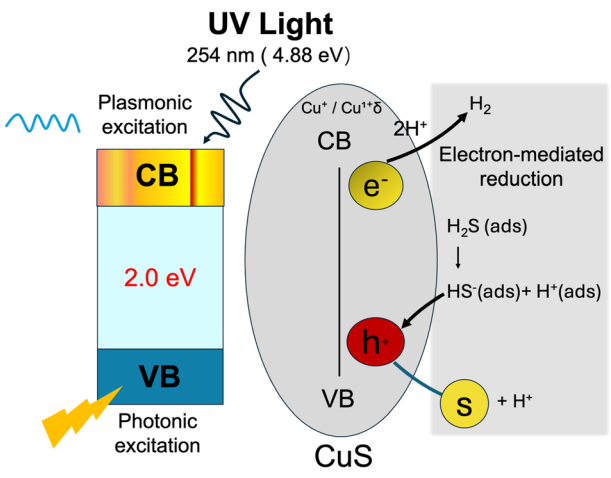


Fig. 11 Schematic illustration of the photocatalytic and plasmon-assisted decomposition of $H_2S$ over CuS under UV illumination.

## 4. Conclusions

This study systematically investigated the photolytic decomposition of $H_2S$ using two UV sources (a UV laser at 220 nm and a Hg lamp at 254 nm), thereby illuminating different reactor systems. Under UV irradiation at wavelengths of 220 nm and 254 nm, remarkable efficiency in $H_2S$ splitting, yielding nearly equimolar hydrogen in the gas phase, was demonstrated. At 220 nm, conversion efficiency of $\sim 8.54 \times 10^{-7}$ of $H_2S$ per joule was achieved. Meanwhile, photolysis experiments at 254 nm yielded conversion efficiency of $\sim 4.4 \times 10^{-9}$ moles of $H_2S$ per joule which demonstrated the significantly higher efficiency of 220 nm wavelength in dissociating H–S bond in $H_2S$ molecules. In flow experiments, at a GHSV = 15 $h^{-1}$ of 15 $h^{-1}$ with a high concentration (5% $H_2S/N_2$), we achieved ~13–16% conversion. The sulfur powder produced during the reaction presents a significant challenge for utilizing the full potential of UV light. However, heating and proper quenching of sulfur can provide a viable solution for photochemical $H_2S$ removal technology.

Incorporating CuS significantly enhanced photocatalytic activity, achieving ~66% $H_2S$ conversion within 60 minutes under 254 nm UV illumination, outperforming photolysis alone (~52%). XPS analysis revealed that copper is predominantly present as $Cu^{+1}$, with higher binding energy contributions attributed to partially oxidized or delocalized $Cu^{1+}\delta$ states. This electronic structure enables localized surface plasmon resonance (LSPR) and stabilizes hot carriers, thereby improving charge separation and reactivity. S 2p spectra further confirmed the formation of elemental sulfur ($S^0$) during the reaction, while XRD of spent catalysts identified crystalline sulfur phases without significant CuS degradation, highlighting structural resilience.

Collectively, these findings highlight the potential of CuS-based photocatalytic systems for sustainable hydrogen and sulfur production from $H_2S$. Addressing sulfur deposition effects and optimizing reactor configurations will be critical for translating this approach into practical, scalable applications. Future research should aim to deepen mechanistic

understanding and refine catalyst design to maximize efficiency and stability in real-world conditions.

## Conflicts of interest

There are no conflicts to declare.

## Data availability

The data supporting the findings of this study, including raw gas chromatographic measurements, XPS spectra, and optical power measurements, are available from the corresponding author upon request.

Supplementary information: Additional supporting figures and videos are provided in the Supplementary Information (SI). See DOI: https://doi.org/10.1039/d5ra04250j.

## Acknowledgements

The authors are grateful for funding from Saudi Aramco (Award no. 5136).

## References

1 S. L. Malone Rubright, L. L. Pearce and J. Peterson, Environmental toxicology of hydrogen sulfide, *Nitric Oxide*, 2017, **71**, 1–13, DOI: 10.1016/j.niox.2017.09.011.

2 M. C. Canela, M. C. Canela, M. C. Canela, R. M. Alberici and W. F. Jardim, Gas-phase destruction of H2S using TiO2/UV-VIS, *J. Photochem. Photobiol., A*, 1998, **112**(1), 73–80, DOI: 10.1016/s1010-6030(97)00261-x.

3 H. A. Elmawgoud, T. M. Elshiekh, M. Abdelkreem, S. A. Khalil and A. M. Alsabagh, Optimization of petroleum crude oil treatment using hydrogen sulfide scavenger, *Egypt. J. Pet.*, 2019, **28**, 161–164, DOI: 10.1016/j.ejpe.2019.02.001.

4 Y. S. Choi, S. Hassani, T. N. Vu, S. Nešić and A. Z. B. Abas, Effect of H2S on the corrosion behavior of pipeline steels in supercritical and liquid CO2 environments, *Corrosion*, 2016, **72**, 999–1009, DOI: 10.5006/2026.

5 M. Abdollahi, and A. Hosseini, Hydrogen Sulfide, in *Encyclopedia of Toxicology*, Elsevier, 2014, pp. 971–974, DOI: 10.1016/B978-0-12-386454-3.00513-3.

6 J. G. Speight, *The Chemistry and Technology of Petroleum*, CRC Press, 2006, DOI: 10.1201/9781420008388.

7 L. Sun and J. Liang, Solubility modeling of hydrogen sulfide in aqueous sodium salt solutions, *Environ. Technol. Innovation*, 2023, **32**, 103334, DOI: 10.1016/j.eti.2023.103334.

8 M. Sassi and A. K. Gupta, Sulfur Recovery from Acid Gas Using the Claus Process and High Temperature Air Combustion (HiTAC) Technology, *Am. J. Environ. Sci.*, 2008, **4**(5), 502–511, DOI: 10.3844/ajessp.2008.502.511.

9 X. Yu, X. Tao, Y. Gao, L. Ding, Y. Wang, G. Yu and F. Wang, Oxygen Vacancy-Mediated Selective $H_2S$ Oxidation over Co-Doped LaFex $Co_{1-x}O_3$ Perovskite, *Catalysts*, 2022, **12**(2), 236, DOI: 10.3390/catal12020236.

10 X. Zhang, G. Dou, Z. Wang, J. Cheng, H. Wang, C. Ma and Z. Hao, Selective oxidation of H2S over V2O5 supported on CeO2-intercalated Laponite clay catalysts, *Catal. Sci. Technol.*, 2013, **3**, 2778–2785, DOI: 10.1039/c3cy00431g.

11 K. Huang, X. Feng, X. M. Zhang, Y. T. Wu and X. B. Hu, The ionic liquid-mediated Claus reaction: A highly efficient capture and conversion of hydrogen sulfide, *Green Chem.*, 2016, **18**, 1859–1863, DOI: 10.1039/c5gc03016a.

12 J. Zhou, Y. Zhao, C. S. Hansen, J. Yang, Y. Chang, Y. Yu, G. Cheng, Z. Chen, Z. He, S. Yu, H. Ding, W. Zhang, G. Wu, D. Dai, C. M. Western, M. N. R. Ashfold, K. Yuan and X. Yang, Ultraviolet photolysis of H2S and its implications for SH radical production in the interstellar medium, *Nat. Commun.*, 2020, **11**, 1547, DOI: 10.1038/s41467-020-15343-4.

13 H. Aljama, Z. Alaithan and A. Almofleh, Catalytic Conversion of $H_2S$ to $H_2$: Challenges and Catalyst Limitations, *J. Phys. Chem. C*, 2023, **127**(19), 9022–9029, DOI: 10.1021/acs.jpcc.3c00903.

14 M. Al Hamadi, S. Ibrahim and A. Raj, Effects of Oxygen Enrichment on Natural Gas Consumption and Emissions of Toxic Gases (CO, Aromatics, and SO2) in the Claus Process, *Ind. Eng. Chem. Res.*, 2019, **58**, 16489–16501, DOI: 10.1021/acs.iecr.9b03408.

15 K. Huang, X. Feng, X. M. Zhang, Y. T. Wu and X. B. Hu, The ionic liquid-mediated Claus reaction: A highly efficient capture and conversion of hydrogen sulfide, *Green Chem.*, 2016, **18**, 1859–1863, DOI: 10.1039/c5gc03016a.

16 X. Zhang, Y. Tang, S. Qu, J. Da and Z. Hao, H2S-selective catalytic oxidation: Catalysts and processes, *ACS Catal.*, 2015, **5**, 1053–1067, DOI: 10.1021/cs501476p.

17 S. Ibrahim, A. Al Shoaibi and A. K. Gupta, Effect of Benzene on Product Evolution in a $H_2S/O_2$ Flame under Claus Condition, *Appl. Energy*, 2015, **145**, 21–26, DOI: 10.1016/j.apenergy.2015.01.094.

18 S. Sinha, A. Raj, A. S. Al Shoaibi and S. H. Chung, Reaction Mechanism for m-Xylene Oxidation in the Claus Process by Sulfur Dioxide, *J. Phys. Chem. A*, 2015, **119**, 9889–9900, DOI: 10.1021/acs.jpca.5b06020.

19 R. K. Rahman, A. Raj, S. Ibrahim, I. M. Khan and N. O. Al Muhairi, Reduction in Natural Gas Consumption in Sulfur Recovery Units through Kinetic Simulation Using a Detailed Reaction Mechanism, *Ind. Eng. Chem. Res.*, 2018, **57**, 1417–1428, DOI: 10.1021/acs.iecr.7b04667.

20 D. Jones, D. Bhattacharyya, R. Turton and S. E. Zitney, Rigorous kinetic modeling and optimization study of a modified claus unit for an Integrated Gasification Combined Cycle (IGCC) power plant with CO 2 capture, *Ind. Eng. Chem. Res.*, 2012, **51**, 2362–2375, DOI: 10.1021/ie201713n.

21 H. Oladipo, A. Yusuf, S. Al Jitan and G. Palmisano, Overview and challenges of the photolytic and photocatalytic splitting of H2S, *Catal. Today*, 2021, **380**, 125–137, DOI: 10.1016/j.cattod.2021.03.021.

22 M. Lou, R. Wang and H. Song, Advances and challenges toward efficient utilization of H2S for H2 production,

*Renewable Sustainable Energy Rev.*, 2024, **199**, 114529, DOI: 10.1016/j.rser.2024.114529.

23 M. Ferree, J. Kosco, F. Laquai, A. Cavazos Sepulveda and D. P. San Roman Alerigi, Solar Fuel Production from Hydrogen Sulfide: An Upstream Energy Perspective, *Adv. Energy Sustainability Res.*, 2023, **4**(8), 2200201, DOI: 10.1002/aesr.202200201.

24 A. Elkhazraji, Q. Wang, M. Monge-Palacios, J. Zou, A. Alshaarawi, A. C. Sepulveda, S. M. Sarathy and A. Farooq, Oxidation of hydrogen sulfide and CO2 mixtures: Laser-based multi-speciation and kinetic modeling, *Chem. Eng. J.*, 2024, **486**, 150421, DOI: 10.1016/j.cej.2024.150421.

25 H. Kiuchi, K. Funaki and T. Tanaka, Thermochemical decomposition of hydrogen sulfide with nickel sulfide, *Metall. Trans. B*, 1983, **14**, 347–352, DOI: 10.1007/BF02654352.

26 K. Garg, M. Kumar, S. Kaur and T. C. Nagaiah, Electrochemical Production of Hydrogen from Hydrogen Sulfide Using Cobalt Cadmium Sulfide, *ACS Appl. Mater. Interfaces*, 2023, **15**, 27845–27852, DOI: 10.1021/acsami.3c01318.

27 Q. Z. Zhang, W. Z. Wang, C. Thille and A. Bogaerts, H2S Decomposition into H2 and S2 by Plasma Technology: Comparison of Gliding Arc and Microwave Plasma, *Plasma Chem. Plasma Process.*, 2020, **40**, 1163–1187, DOI: 10.1007/s11090-020-10100-3.

28 M. Dan, S. Yu, Y. Li, S. Wei, J. Xiang and Y. Zhou, Hydrogen sulfide conversion: How to capture hydrogen and sulfur by photocatalysis, *J. Photochem. Photobiol., C*, 2020, **42**, 100339, DOI: 10.1016/j.jphotochemrev.2019.100339.

29 N. Biihler, K. Meier and J.-F. Reber, Photochemical Hydrogen Production with Cadmium Sulfide Suspensions, *J. Phys. Chem.*, 1984, **88**(15), 3261–3268.

30 V. Preethi and S. Kanmani, Photocatalytic hydrogen production, *Mater. Sci. Semicond. Process.*, 2013, **16**, 561–575, DOI: 10.1016/j.mssp.2013.02.001.

31 M. Takase, S. Furukawa, S. Matsuda, K. I. Nishimori and Y. Kanda, Development of Hydrogen Recycling Systems for Petroleum Refiner-2 ies: Hydrogen Sulfide Decomposition Using Titania Photocatalyst, *J. Jpn. Pet. Inst.*, 2018, **61**, 361–364, DOI: 10.1627/jpi.61.361.

32 H. Ye, W. Xing, F. Zhao, J. Wang, C. Yang, Y. Hou, J. Zhang, J. C. Yu and X. Wang, Sabatier Optimal of Mn-N4 Single Atom Catalysts for Selective Oxidative Desulfurization, *Angew. Chem., Int. Ed.*, 2025, **64**(7), e202419630, DOI: 10.1002/anie.202419630.

33 S. Chakraborty, T. L. Jackson, M. Ahmed and M. H. Thiemens, Sulfur isotopic fractionation in vacuum UV photodissociation of hydrogen sulfide and its potential relevance to meteorite analysis, *Proc. Natl. Acad. Sci. U. S. A.*, 2013, **110**, 17650–17655, DOI: 10.1073/pnas.1213150110.

34 J. Steadman, S. K. Cole and T. Baer, Visible and ultraviolet resonance enhance multiphoton ionization photoelectron spectroscopy of H2S in the one-photon wavelength region 143-158 nm, *J. Chem. Phys.*, 1988, **89**, 5498–5506, DOI: 10.1063/1.455602.

35 J. Hong, C. Xu, B. Deng, Y. Gao, X. Zhu, X. Zhang and Y. Zhang, Photothermal Chemistry Based on Solar Energy: From Synergistic Effects to Practical Applications, *Adv. Sci.*, 2022, **9**(3), 2103926, DOI: 10.1002/advs.202103926.

36 J. S. Jang, H. Gyu Kim, P. H. Borse and J. S. Lee, Simultaneous hydrogen production and decomposition of H2 S dissolved in alkaline water over CdS - TiO2 composite photocatalysts under visible light irradiation, *Int. J. Hydrogen Energy*, 2007, **32**, 4786–4791, DOI: 10.1016/j.ijhydene.2007.06.026.

37 Y. Gilboa, Y. Alfiya, S. Sabach, E. Friedler and Y. Dubowski, $H_2S$ Removal from Groundwater by Chemical Free Advanced Oxidation Process Using UV-C/VUV Radiation, *Molecules*, 2021, **26**(13), 4016, DOI: 10.3390/molecules26134016.

38 J. Xu, C. Li, P. Liu, D. He, J. Wang and Q. Zhang, Photolysis of low concentration H2S under UV/VUV irradiation emitted from high frequency discharge electrodeless lamps, *Chemosphere*, 2014, **109**, 202–207, DOI: 10.1016/j.chemosphere.2014.01.065.

39 Y. Uesugi, H. Nagakawa and M. Nagata, Highly Efficient Photocatalytic Degradation of Hydrogen Sulfide in the Gas Phase Using Anatase/TiO2(B) Nanotubes, *ACS Omega*, 2022, **7**, 11946–11955, DOI: 10.1021/acsomega.1c07294.

40 H. G. Baldovi, J. Albero, B. Ferrer, D. Mateo, M. Alvaro and H. García, Gas-Phase Photochemical Overall H2S Splitting by UV Light Irradiation, *ChemSusChem*, 2017, **10**, 1996–2000, DOI: 10.1002/cssc.201700294.

41 K. Vikrant, K. H. Kim and A. Deep, Photocatalytic mineralization of hydrogen sulfide as a dual-phase technique for hydrogen production and environmental remediation, *Appl. Catal., B*, 2019, **259**, 118025, DOI: 10.1016/j.apcatb.2019.118025.

42 J. Ali, W. Jiang, A. Shahzad, J. Ifthikar, X. Yang, B. Wu, D. T. Oyekunle, W. Jia, Z. Chen, L. Zheng and Z. Chen, Isolated copper ions and surface hydroxyl groups as a function of non-redox metals to modulate the reactivity and persulfate activation mechanism of spinel oxides, *Chem. Eng. J.*, 2021, **425**, 130679, DOI: 10.1016/j.cej.2021.130679.

43 S. Blaseio, C. Dosche, M. Rahaman, K. Kiran, A. Dworzak, B. Mahrt, P. Broekmann, A. Dutta and M. Oezaslan, Impact of $Cu^+$ and $Cu^{2+}$ species on the oxide-metal transition processes of $Cu_xO$ foams during the $CO_2RR$ probed by operando Quick-XAS, *J. Mater. Chem. A*, 2024, **12**, 28177–28192, DOI: 10.1039/d4ta02217c.

44 Y. Fu, Z. Wu, Y. Yuan, P. Chen, L. Yu, L. Yuan, Q. Han, Y. Lan, W. Bai, E. Kan, C. Huang, X. Ouyang, X. Wang, J. Zhu and J. Lu, Switchable encapsulation of polysulfides in the transition between sulfur and lithium sulfide, *Nat. Commun.*, 2020, **11**(1), 1–10, DOI: 10.1038/s41467-020-14686-2.

45 X. Deng, A. Verdaguer, T. Herranz, C. Weis, H. Bluhm and M. Salmeron, Surface chemistry of Cu in the presence of CO2 and H 2O, *Langmuir*, 2008, **24**, 9474–9478, DOI: 10.1021/la8011052.

46 W. Van Der Stam, S. Gudjonsdottir, W. H. Evers and A. J. Houtepen, Switching between Plasmonic and Fluorescent Copper Sulfide Nanocrystals, *J. Am. Chem. Soc.*, 2017, **139**, 13208–13217, DOI: **10.1021/jacs.7b07788**.
47 Y. Xie, W. Chen, G. Bertoni, I. Kriegel, M. Xiong, N. Li, M. Prato, A. Riedinger, A. Sathya and L. Manna, Tuning and Locking the Localized Surface Plasmon Resonances of CuS (Covellite) Nanocrystals by an Amorphous CuPdxS Shell, *Chem. Mater.*, 2017, **29**, 1716–1723, DOI: **10.1021/acs.chemmater.6b05184**.